

Ab initio Molecular Dynamics Simulations of the Initial Stages of Solid-electrolyte Interphase Formation on Lithium Ion Battery Graphitic Anodes

Kevin Leung^{1*} and Joanne L. Budzien²

¹*Surface and Interface Sciences Department, MS 1415, Sandia National Laboratories, Albuquerque, New Mexico 87185, USA; kleung@sandia.gov*

²*Department of Physics and Engineering Frostburg State University, Frostburg, MD 21532, USA*
(Dated: September 10, 2018)

The decomposition of ethylene carbonate (EC) during the initial growth of solid-electrolyte interphase (SEI) films at the solvent-graphitic anode interface is critical to lithium ion battery operations. *Ab initio* molecular dynamics simulations of explicit liquid EC/graphite interfaces are conducted to study these electrochemical reactions. We show that carbon edge terminations are crucial at this stage, and that achievable experimental conditions can lead to surprisingly fast EC breakdown mechanisms, yielding decomposition products seen in experiments but not previously predicted.

Improving the fundamental scientific understanding of lithium ion batteries^{1–3} is critical for electric vehicles and efficient use of solar and wind energy. A key limitation in current batteries is their reliance on passivating solid electrolyte interphase (SEI) films on graphitic anode surfaces.^{1–5} Upon first charging of a pristine battery, the large negative potential applied to induce Li⁺ intercalation into graphite decomposes ethylene carbonate (EC, Fig. 1) molecules in the solvent, yielding a self-limiting, 30–50 nm thick, passivating SEI layer containing Li₂CO₃, lithium ethylene dicarbonate ((CH₂CO₃Li)₂),^{2,4–6} and salt decomposition products. C₂H₄ and CO gases have also been detected^{7,8} and shown to come from EC.⁹ Similar reactions occur during power cycling when the SEI film cracks and graphite is again exposed to EC.² If instead the solvent is pure propylene carbonate (PC), a stable SEI film does not materialize^{1,2} and the battery fails. Our work shows that novel mechanisms for the initial stages of SEI-growth at electrode-electrolyte interfaces can be simulated within time scales accessible to *ab initio* molecular dynamics (AIMD),¹⁰ which have successfully modelled liquid-solid interfaces.¹¹ AIMD is likely also applicable to shed light on cosolvent/additives which must decompose more readily than EC to alter and improve SEI structure, Li⁺ transport, and passivating properties.^{1,2}

EC-decomposition mechanisms under electron-rich conditions have been proposed (e.g., Refs. 4,5) and investigated using gas cluster Density Functional Theory calculations with and without dielectric continuum approximation of the liquid environment.^{12–15} Thus “EC[−]”, coordinated to Li⁺ or otherwise, has been predicted to undergo ethylene carbon (C_E)-oxygen (O₁) bond cleavage to form a more stable radical anion (Figs. 1a-b). The potential energy barrier involved is at least 0.33 eV.^{12,14} Carbonyl carbon (C_C)-O₁ bond-“breaking” (or elongation) in the gas phase EC[−]-Li⁺ complex yields a lower barrier, but metastable products.¹⁴

Unlike these previous work, AIMD simulations can include explicit liquid state environments and EC/graphite interfaces. Unlike classical force field-based simulations,^{16,17} AIMD accounts for covalent bond-breaking. We apply the VASP code,^{18,19} the Perdew-

Burke-Ernzerhof (PBE) functional,²⁰ Γ -point Brillouin zone sampling, 400 eV planewave energy cutoff, tritium masses for all protons to allow Born-Oppenheimer dynamics time steps of 1 fs, and a 10^{−6} eV energy convergence criterion. The hybrid PBE0 functional,^{21,22} more accurate in many cases, is used for spot checks. A Nose thermostat maintains the temperature at T=450 K to avoid EC freezing. A uniform neutralizing background charge is imposed on systems with net charges.²³ Non-adiabatic quantum effects,²⁴ not generally evoked in EC-breakdown reactions,^{12–15} are neglected and will be examined in the future. Some gas phase calculations are also conducted using the Gaussian suite of programs and a 6-311++G(d,p) basis.²⁵

We first consider liquid EC to motivate subsequent breakdown products at the EC-graphite interface. A 17 ps trajectory with 32 EC molecules and a Li⁺, but no excess e[−], is conducted in a (15.24 Å)³ simulation cell, corresponding to the experimental 1.32 g/cc EC density.¹⁷ Integrating over the first peak of the pair correlation function ($g(r)$, Fig. 1c) between Li⁺ and O atoms yields a solvation number $N_{EC} = 4.0$, in agreement with a classical force field prediction^{17,26} but slightly smaller than the Raman value of 4.9.²⁷

Next we add an excess e[−] to three randomly chosen configurations along the Li⁺-32 EC trajectory and restart AIMD. (Liquid state chemical reactions require multiple initial conditions to account for the disorder.) The 9.7 kcal/mol C_E-O₁ cleavage barrier previously predicted¹² implies 10^{−9}s lifetimes at T=450 K if one assumes a vibrational prefactor of 10^{−13}s^{−1}. The $g(r)$ from one 20 ps AIMD run is indeed consistent with this prediction (Fig. 1c). An excess electron is trapped on an EC near the Li⁺. Its N_{EC} averages to 3.3; no bond breaking, even of the C_C-O₁ type,¹⁴ is observed. An AIMD snapshot confirms that the excess e[−] is trapped on an EC[−]-Li⁺ complex,¹² at the carbonate end (Fig. 1d).

In contrast, two other starting configurations lead to a new mechanism: a C_E-O₁ bond breaks irreversibly in two distinct EC molecules outside the Li⁺ first solvation shell within a surprisingly short 0.8 ps (Fig. 2a-b). Here the excess e[−] may have avoided the Li⁺ vicinity because the Li⁺ N_{EC} may need to spontaneously decrease

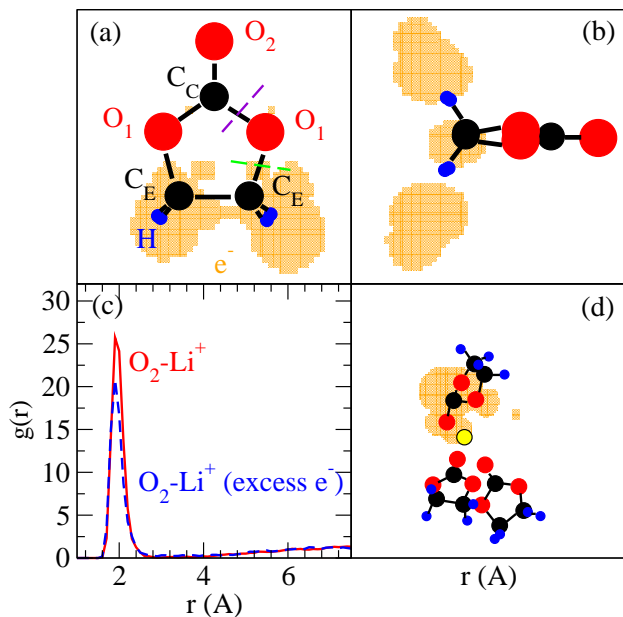


FIG. 1: Black, red, blue, and yellow spheres: C, O, H, and Li. Orange shading: regions of spin (i.e., excess e^-) density $\rho_s > 8 \times 10^{-3} |e|\text{\AA}^{-3}$. (a) & (b) Isolated EC^- . Green and violet lines depict two breakdown modes; the latter is observed only with explicit treatment of liquid EC (see text). (c) $g(r)$ between Li^+ and EC O_2 site for systems with and without excess e^- . (d) Snapshot of Li^+ coordinated to intact EC^- and two other EC molecules (other EC in the liquid omitted).

to accommodate an electron (Fig. 1c), leading to an kinetic barrier. This mechanism may dominate in high excess e^- concentration ($[e^-]$) regions near the anode if most Li^+ there have already complexed with EC^- . While the PBE functional we use might slightly underestimate barriers compared to hybrid functionals,^{12,14} it still predicts a barrier of 0.37 eV for isolated EC^- and a free energy barrier of 0.33 eV when a dielectric continuum solvation is added. (See the electronic supporting information, ESI.) Furthermore, gas phase EC^- is not observed to crack within a 7 ps AIMD trajectory. Thus explicit treatment of solvent EC molecules, which have large dipole moments, appears responsible for the fast reaction rate. Given the use of the tritium masses and the slightly lower PBE functional reaction barriers, we should focus on relative (not absolute) time scales of different mechanisms, not absolute values.

The disparity between gas and solution phase rates likely arises from the repulsive electron affinity of gas phase EC^- .¹² While electronic structure calculations can impose a metastable isolated “ EC^- ,” the excess e^- lies *outside* the molecule (Fig. 1b); the $\text{C}_E\text{-O}_1$ anti-bonding orbital is not occupied and bond-breaking is not facilitated. In contrast, AIMD/PBE simulations predict that, in liquid EC, the excess e^- is initially delocalized *within* one or more EC molecules, unlike in water where excess e^- occupies intermolecular spaces stabilized by

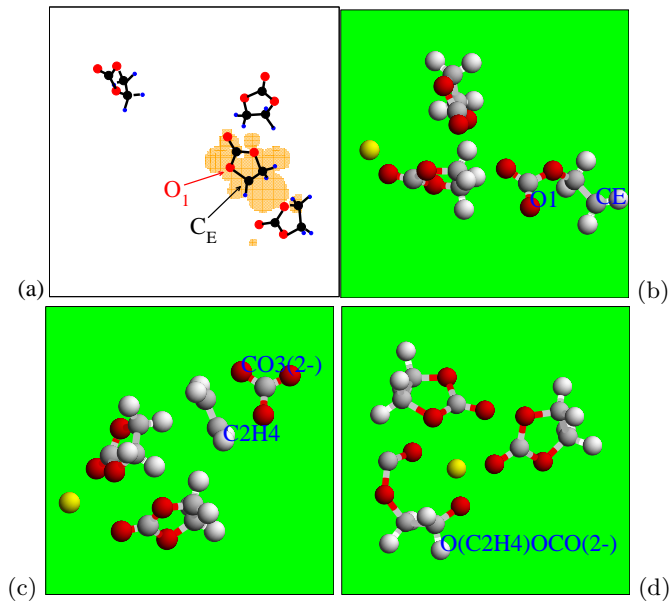


FIG. 2: (a) In this snapshot, substantial e^- density resides on the EC with a $\text{C}_E\text{-O}_1$ bond about to break. (b) $\text{C}_E\text{-O}_1$ bond breaks in the EC^- soon afterwards. (c) & (d) $\text{EC}^- + e^- \rightarrow \text{C}_2\text{H}_4 + \text{CO}_3^{2-}$ or $\text{O}(\text{C}_2\text{H}_4)\text{OCO}^{2-}$, after 50 fs and 1.0 ps respectively. Only a few select EC are shown; the colors are as in Fig. 1 except that C and H are grey and white in panels (b)-(d).

hydrogen-bond donors.²⁴ When instantaneous favorable molecular geometries localize the e^- on one EC and substantially populates orbitals on C and O atoms (Fig. 2a), bond-breaking pathways with rates different from that in the gas phase emerge. Using a EC liquid snapshot, we confirm that the spatial distribution of excess e^- computed using PBE and PBE0 functionals are qualitatively similar.²⁶ This behavior depends on the LUMO (lowest unoccupied molecular orbital) level; while PBE and PBE0 predicts gas phase HOMO (highest occupied MO)-LUMO gaps of 6 eV and 8.2 eV respectively, the PBE0 LUMO energy level is higher by only 0.45 eV.

Doubling $[e^-]$ by adding another spin-antiparallel e^- to the Fig. 2b liquid configuration yields a $\text{C}_2\text{H}_4/\text{CO}_3^{2-}$ pair within 50 fs (Fig. 2c). Starting with the $\text{EC}^- \text{-Li}^+$ complex in Fig. 1d and adding an e^- leads to $\text{C}_E\text{-O}_1$ bond cleavage and a $\text{O}(\text{C}_2\text{H}_4)\text{OCO}^{2-}$ instead (Fig. 2d; see ESI for charge state analyses). This bond was previously shown to be the weaker bond when even one electron is added to EC^- .¹⁴ The latter fast 2- e^- mechanism is not seen without explicit solvent.¹⁵

Having re-examined breakdown in liquid EC, we turn to interfacial reactions, the main thrust of this work. Four layers of Li-intercalated graphite are optimized in a periodically replicated $29.74 \times 14.97 \times 15.06 \text{\AA}^3$ cell with zig-zag edges exposed (Fig. 3). The box size preserves the density of the liquid region containing 32 EC after accounting for the van der Waals radii of the electrode atoms. Dangling σ -orbitals on edge carbon atoms should

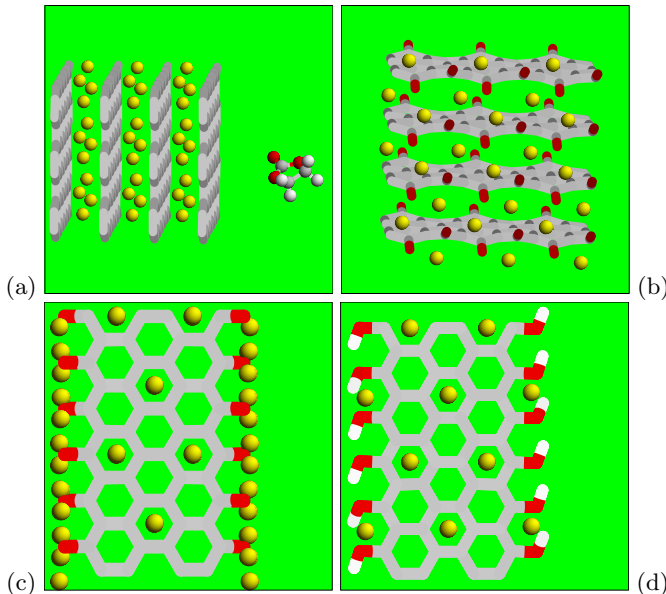


FIG. 3: (a) Basal plane LiC_6 plane ($\text{C}_{288}\text{Li}_{36}$); (b)&(c) $\text{C}=\text{O}$ edge ($\text{C}_{192}\text{O}_{48}\text{Li}_{72}$), side and top views; in (b), only the outermost layer of Li chelated to 3 O atoms each are depicted; (d) $\text{C}-\text{OH}$ edge ($\text{C}_{192}\text{O}_{48}\text{H}_{48}\text{Li}_{32}$). $\text{C}-\text{H}$ edges (not shown) have no Li at edge sites. The stick figures depict graphite C, O, and H atoms; color scheme as in Fig. 2.

be terminated with hydroxyl ($\text{C}-\text{OH}$), quinone ($\text{C}=\text{O}$), carboxylic acid (COOH) functional groups, and/or protons; only the first three are electrochemically active.²⁸ We perform AIMD simulations on $\text{C}=\text{O}$, $\text{C}-\text{OH}$, and $\text{C}-\text{H}$ terminated LiC_6 interfaces, and use static calculations on the basal (0001) plane (Fig. 3a), impervious to Li^+ , as a reference. Constant voltage conditions^{4,5} are not yet feasible with AIMD. Instead, our LiC_6 stoichiometry²⁹ in the slab interior mimics a fully-charged battery anode. To some extent our simulation is akin to “immersing” SEI-free LiC_6 , pre-formed at low voltage, into EC liquid; this is analogous to the conditions for SEI growth on Li metal, which yield EC-specific SEI similar to those on graphitic anodes.⁴

The optimal geometry when Li occupy all $\text{C}=\text{O}$ edge sites is depicted in Fig. 3b and 3c. Each Li is chelated to two and one O atoms on successive graphite sheets (3 oxygens total), with edge $\text{C}=\text{O}$ bonds tilted out of the graphite planes to maximize interaction with Li. The mean Li-O distance is 1.98 Å. The Li chemical potential (μ_{Li}) computed by randomly removing an edge Li atom is below -2.4 eV, less than the $\mu_{\text{Li}}=-2.0$ eV in the basal slab (Fig. 3a), suggesting the number of Li atoms is appropriate. For $\text{C}-\text{OH}$ edge LiC_6 , when Li occupies every sixth edge site chelated with 2 O atoms on successive graphite sheets (4 total, Fig. 3d), μ_{Li} is too high at -1.7 eV; too many Li are present. Nevertheless, this structure is considered because mixed $\text{C}=\text{O}/\text{C}-\text{OH}$ edges provide a proton source. The band offsets between these model electrodes and isolated EC molecules are more favorable for electron transfer than that associated with

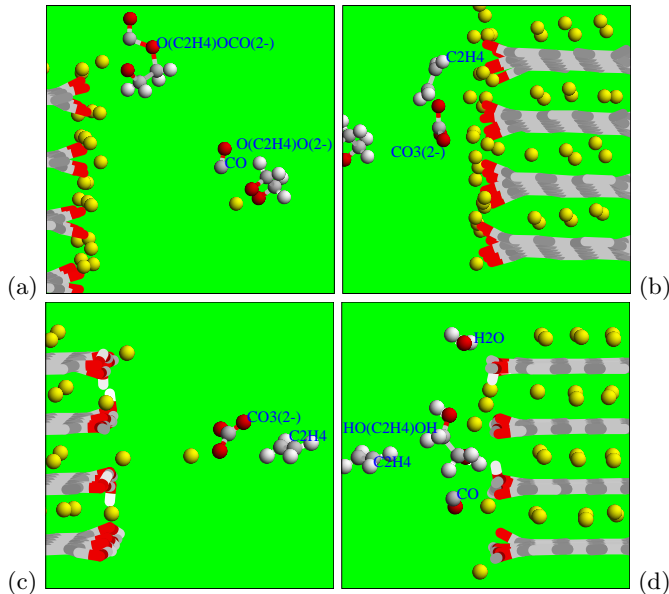


FIG. 4: EC breakdown products near the end of AIMD runs. Intact EC (not shown) fill the empty spaces. (a) $\text{C}=\text{O}$ edge: a $\text{OC}_2\text{H}_4\text{OCO}_2^-$, and a $\text{CO}/\text{OC}_2\text{H}_4\text{O}_2^-$ pair (near a Li^+ away from surface). (b) $\text{C}=\text{O}$ (other surface): $\text{CO}_3^{2-}/\text{C}_2\text{H}_4$. (c) $\text{C}-\text{OH}$ edge: $\text{CO}_3^{2-}/\text{C}_2\text{H}_4$ pair near a Li^+ away from surface. (d) $\text{C}-\text{OH}$ (other surface): $\text{CO}/\text{HOC}_2\text{H}_4\text{OH}$, and a H_2O from disproportionation of 3 $\text{C}-\text{OH}$. Color scheme is as in Fig. 3.

basal plane termination; this is shown in the ESI.

AIMD simulations confine 32 EC between the $\text{C}=\text{O}$ edge terminated LiC_6 surfaces (Fig. 3c);²³ in addition to the Li at the $\text{C}=\text{O}$ edges, an extra Li^+ resides in the liquid region. Figures 4a-b and Table 1 show that e^- transfers from the initially charge-neutral LiC_6 into EC to form a $\text{C}_2\text{H}_4/\text{CO}_3^{2-}$ pair (C_E-O_1 cleavage), a $\text{CO}/\text{O}(\text{C}_2\text{H}_4)\text{O}_2^-$ pair, and a $\text{O}(\text{C}_2\text{H}_4)\text{OCO}_2^-$ (C_C-O_1 cleavages). The last moiety may ultimately crack into CO and $\text{O}(\text{C}_2\text{H}_4)\text{O}_2^-$. The $-2|e|$ charge states are confirmed in the ESI. In reactions occurring at electrode surfaces, e^- most likely flows directly to the decomposing EC’s coordinated to surface Li’s without becoming first delocalized in the liquid. As such, this mechanism should not strongly depend on the EC liquid density or the simulation cell size. EC breakdown also occurs in the liquid region where the dianionic products can bind to a Li^+ . In both cases, the products are consistent with $2-e^-$ addition to liquid EC (Figs. 2c & d), except that CO formation has not occurred there yet. Future work will consider counterions in the electric double layer, which however equilibrate at timescales much slower than the observed reactions and are neglected herein.

For the $\text{C}-\text{OH}$ edge, both $\text{C}_2\text{H}_4 + \text{CO}_3^{2-}$ (Fig. 4c) and $\text{CO} + \text{O}(\text{C}_2\text{H}_4)\text{O}_2^-$ (Fig. 4d) products emerge in picoseconds. The $\text{O}(\text{C}_2\text{H}_4)\text{O}_2^-$ then extracts H^+ from the electrode to form ethylene glycol, which has been used as the chemical precursor (alongside carbonates) to *synthesize* $(\text{CH}_2\text{CO}_3\text{Li})_2$ outside battery settings.⁶ To our knowledge, CO products, observed in battery charging

run	edge	spin	t (ps)	CO_3^{2-}	$\text{OC}_2\text{H}_4\text{O}^{2-}$	$\text{OCOC}_2\text{H}_4\text{O}^{2-}$
1	C=O	singlet	7.0	1	1	1
2	C-OH	singlet	7.0	1	1	0
3	C-OH	triplet	6.8	2	0	1
4	C-H	singlet	7.0	0	0	0

TABLE I: EC decomposition products in interfacial simulations. t exclude a 3.5 ps equilibration period during which an extra +4 $|e|$ charge is imposed to hinder EC breakdown. In Run 2, $\text{OC}_2\text{H}_4\text{O}^{2-}$ extracts two protons from C-OH groups to form ethylene glycol; a $\text{OCHOC}_2\text{H}_4\text{OH}$ is formed in Run 3.

experiments,^{7,9} have not been predicted in calculations in the absence of explicit solvents.¹²⁻¹⁵

A spin-polarized triplet spin simulation yields qualitatively similar conclusions (Table 1). In contrast, no EC decomposition is observed at the H-edge interface in 7 ps. The edge dependences are consistent with their known electrochemical activities,²⁸ but are seldom discussed in battery studies because the initial carbon edges become masked by SEI formation.

Our novel predictions suggest the following mechanism for initial SEI growth. Fast EC decomposition initiates at graphite edge regions rich in oxidized sites.³⁰ Both $\text{C}_E\text{-O}_1$ and $\text{C}_C\text{-O}_1$ cleavages occur, yielding CO_3^{2-} and $\text{OC}_2\text{H}_4\text{O}^{2-}$ respectively. $\text{OC}_2\text{H}_4\text{O}^{2-}$, or $\text{HOC}_2\text{H}_4\text{OH}$ if a proton source exists, potentially reacts with CO_2 or CO_3^{2-} at longer time scales to form $(\text{CH}_2\text{CO}_3\text{Li})_2$,⁶ a main SEI component. $\text{C}_C\text{-O}_1$ cleavage and $\text{OC}_2\text{H}_4\text{O}^{2-}$ products (Fig. 1a) are facilitated by Li^+ and other ionic products coordinating to carbon edges. However, slower

e^- transfer to the solvent may mandate different decomposition mechanisms at later stages of SEI growth.³⁻⁵

In conclusion, AIMD simulations can yield new insights concerning ethylene carbonate decomposition in electron-rich anode regions. With explicit treatment of the EC liquid environment, an excess electron can induce EC decomposition within AIMD timescales. On pristine graphitic electrodes, carbon edge terminations strongly affect EC breakdown. C=O edges give strong driving forces and support two EC decomposition pathways, yielding both C_2H_4 and CO gas and ionic products. CO evolution, observed in experiments,⁹ is predicted for the first time. Although our reported time scales may be somewhat affected by the DFT method used, the reactions pertinent to initial stages of SEI growth are surprisingly fast, which potentially opens the way for the versatile AIMD method to investigate the decomposition mechanisms of other solvent or additive molecules.³¹

We thank John Sullivan, David Ingersoll, Kevin Zavadi, Kang Xu, and Perla Balbuena for useful discussions. This work was supported by the Department of Energy under Contract DE-AC04-94AL85000. Sandia is a multiprogram laboratory operated by Sandia Corporation, a Lockheed Martin Company, for the U.S. Department of Energy. KL was partly supported by Nanostructures for Electrical Energy Storage, an Energy Frontier Research Center funded by the U.S. Department of Energy, Office of Science, Office of Basic Energy Sciences under Award Number DESC0001160. The electronic supporting information is available at <http://www.rsc.org>.

¹ *Advances in lithium-ion batteries*, ed. W.A. van Schalkwijk and B. Scrosati (Kluwer, New York, 2002).

² *Lithium-ion batteries: solid-electrolyte interphase*, ed. Y. Wang and P.B. Balbuena (Imperial College, London, 2004).

³ K. Xu, *Chem. Rev.*, 2004, **104**, 4303.

⁴ D. Aurbach, Y. Ein-Eli, O. Chusid, Y. Carmeli, M. Babai, and H. Yamin, *J. Electrochem. Soc.*, 1994, **141**, 603; D. Aurbach, B. Markovsky, A. Shechter, Y. Ein-Eli, and H. Cohen, *ibid.*, 1996, **143**, 3809.

⁵ P. Arora, R. E. White, and M. Doyle, *J. Electrochem. Soc.*, 1998, **145**, 3647.

⁶ G.V. Zhuang, K. Xu, H. Yang, T.R. Jow, and P. N. Ross Jr., *J. Phys. Chem. B*, 2005, **109**, 17567.

⁷ H. Yoshida, T. Fukunaga, T. Hazama, M. Terasaki, M. Mizutani, and M. Yamachi, *J. Power Sources*, 1997, **68**, 311.

⁸ Z. Ogumi, A. Sano, M. Inaba, and T. Abe, *J. Power Sources*, 2001, **97-98**, 156.

⁹ M. Onuki, S. Kinoshita, Y. Sakata, M. Yanagidate, Y. Otake, M. Ue, and M. Deguchi, *J. Electrochem. Soc.* 2008, **155**, A794.

¹⁰ R. Car and M. Parrinello, *Phys. Rev. Lett.*, 1985, **55**, 2471.

¹¹ G. Cicero, J.C. Grossman, E. Schwegler, F. Gygi, and G. Galli, *J. Am. Chem. Soc.*, 2008, **130**, 1871; F. Schif-

mann, J. Hutter, and J. VandeVondele, *J. Phys. Condens. Matter*, 2008, **20**, 064206; N.N. Nair, E. Schreiner, and D. Marx, *J. Am. Chem. Soc.*, 2008, **130**, 14148; L. Liu, M. Krack, and A. Michaelides, *J. Am. Chem. Soc.*, 2008, **130**, 8572; K. Leung, I.M.B Nielsen, and L.J. Criscenti, *J. Am. Chem. Soc.* 2009, **131**, 18358.

¹² Y. Wang, S. Nakamura, M. Ue, and P. B. Balbuena, *J. Am. Chem. Soc.*, 2001, **123**, 11708.

¹³ Y. Wang and P. B. Balbuena, *J. Phys. Chem. B*, 2002, **106**, 4486; *Int. J. Quant. Chem.*, 2005, **102**, 724.

¹⁴ Y.-K. Han and S.U. Lee, *Theor. Chem. Acc.*, 2004, **112**, 106.

¹⁵ J.M. Vollmer, L.A. Curtiss, D.R. Vissers, and K. Amine, *J. Electrochem. Soc.*, 2004, **151**, A178.

¹⁶ O. Borodin and G.D. Smith, *J. Phys. Chem. B*, 2006, **110**, 4971.

¹⁷ T. Li and P.B. Balbuena, *J. Electrochem. Soc.*, 1999, **146**, 3613; A. Marquez and P. B. Balbuena, *J. Electrochem. Soc.*, 2001, **148**, A624.

¹⁸ G. Kresse and J. Furthmüller, *Phys. Rev. B*, 1996, **54**, 11169; *Comput. Mater. Sci.*, 1996, **6**, 15.

¹⁹ G. Kresse and D. Joubert, *Phys. Rev. B*, 1999, **59**, 1758.

²⁰ J.P. Perdew, K. Burke, and M. Ernzerhof, *Phys. Rev. Lett.*, 1996, **77**, 3865.

²¹ C. Adamo and V. Barone, *J. Chem. Phys.*, 1999, **110**,

- 6158; M. Ernzerhof and G. E. Scuseria, *J. Chem. Phys.*, 1999, **110**, 5029.
- ²² PBE0 calculations apply VASP 5.2: J. Paier, M. Marsman, and G. Kresse, *J. Chem. Phys.*, 2007, **127**, 024103.
- ²³ AIMD trajectories are initialized using equilibrated classical force fields¹⁷ generated configurations. When pre-equilibrating EC-LiC₆ interfaces, all atoms in the solid are frozen. During AIMD interfacial runs, the C, O, and H atoms at the graphite edge and all Li atoms can move. The costliest, 7 ps spin-polarized interfacial trajectory took 10⁵ cpu-hours on Intel processors.
- ²⁴ F.J. Webster, J. Schnitker, M.S. Friedrichs, R.A. Friesner, and P.J. Rossky, *Phys. Rev. Lett.*, 1991, **66**, 3172.
- ²⁵ M.J. Frisch, *et al.*, Gaussian 03 (Revision C.02), Gaussian Inc., Wallingford, CT, 2004. See the electronic supporting data (ESI) for more details.
- ²⁶ J.-M. Yu, P.B. Balbuena, J. Budzien and K. Leung, *J. Electrochem. Soc.* (submitted).
- ²⁷ S.A. Hyodo and K. Okabayashi, *Electrochem. Acta*, 1989, **34**, 1551.
- ²⁸ R.L. McCreery, *Chem. Rev.*, 2008, **108**, 2646.
- ²⁹ N.A.W Holzwarth, S. G. Louie, and S. Rabii, *Phys. Rev. B*, 1983, **28**, 1013.
- ³⁰ Y. Ein-Eli, *Solid-State Lett.* 1999, **2**, 212; D. Aurbach, H. Teller, and E. Levi, *J. Electrochem. Soc.* 2002, **149**, A1255.
- ³¹ Notes added in proofs: preliminary AIMD/PBE0 simulations yield a lower tendency towards two-electron induced CO formation in EC liquid (Fig. 2d),²⁶ but show that the pertinent C-O bond breaking readily occurs at the electrolyte-electrode interface.